

M easurement of the proton and deuteron structure functions, F_2^p and F_2^d , and of the ratio $R = \frac{F_2^p}{F_2^d}$

THE NEW MUON COLLABORATION (NMC)

Bielefeld University¹⁺, Freiburg University²⁺, Max-Planck Institut für Kernphysik, Heidelberg³⁺,
Heidelberg University⁴⁺, Mainz University⁵⁺, Mons University⁶, Nuchatel University⁷, Nikhef⁸⁺⁺, Saclay
DAPNIA/SPP⁹, University of California, Santa Cruz¹⁰, Paul Scherrer Institut¹¹, Torino University and
INFN Torino¹², Uppsala University¹³, Soltan Institute for Nuclear Studies, Warsaw¹⁴, Warsaw University¹⁵

M. Amendo^{12a)}, A. Arvidson¹³, B. Badelek^{13;15}, M. Ballintijn⁸, G. Baum¹, J. Beaufays⁸,
I.G. Bärd^{3;8b)}, P. Björkholm¹³, M. Botje^{11c)}, C. Brøggini^{7d)}, W. Brückner³, A. Brull^{2e)},
W. Burger^{11f)}, J. Ciborowski¹⁵, R. van Dantzig⁸, A. Dyring¹³, H. Engelien², M. I. Ferrero¹²,
L. Fluri⁷, U. Gaul³, T. Granier^{9g)}, M. Grosse-Perdikam^{2h)}, D. von Harrach³ⁱ⁾,
M. van der Heijden⁸, C. Heusch¹⁰, Q. Ingram¹¹, M. de Jong^{8b)}, E. M. K. Abu³ⁱ⁾, R. Kaiser²,
T. J. K. et al.⁸, F. Klein^{5j)}, S. Kullander¹³, U. Landgraf², T. Lindqvist¹³, G. K. M. allot⁵, C. M. Ariotti^{12k)},
G. van Middelkoop⁸, A. M. Iisztajn⁹, Y. Mizuno^{3l)}, A. M. Ost^{3m)}, A. M. Ucklich³, J. Nassalski¹⁴,
D. Nowotny³, J. Oberski⁸, A. Paic⁷, C. Peroni¹², B. Povh^{3;4}, K. Przytz¹³ⁿ⁾, R. Rieger⁵, K. Rith^{3o)},
K. Rohrich^{5p)}, E. Rondio^{14b)}, L. Ropelowski^{15b)}, A. Sandacz¹⁴, D. Sanders^{9j)}, C. Scholz³, R. Seitz^{5r)},
F. Sever^{1;8s)}, T. A. Shibata^{4t)}, M. Siebler¹, A. Simonon^{3u)}, A. Staiano¹², M. Szleper¹⁴, W. Tarczala^{14v)},
Y. Tzamouranis^{3q)}, M. Vérchaux⁹, J. L. Vuilleumier⁷, T. Walcher⁵, R. Windmolders⁶, A. Witmann²,
K. Zaremba^{14v)}, F. Zetsche^{3w)}

(submitted to Nuclear Physics)

Abstract

The muon-proton and muon-deuteron inclusive deep inelastic scattering cross sections were measured in the kinematic range $0.002 < x < 0.60$ and $0.5 < Q^2 < 75 \text{ GeV}^2$ at incident muon energies of 90, 120, 200 and 280 GeV. These results are based on the full data set collected by the New Muon Collaboration, including the data taken with a small angle trigger. The extracted values of the structure functions F_2^p and F_2^d are in good agreement with those from other experiments. The data cover a sufficient range of y to allow the determination of the ratio of the longitudinally to transversely polarised virtual photon absorption cross sections, $R = \frac{F_2^p}{F_2^d}$, for $0.002 < x < 0.12$. The values of R are compatible with a perturbative QCD prediction; they agree with earlier measurements and extend to smaller x .

| | | | | | | | | {

For footnotes see next page.

- + Supported by Bundesministerium für Bildung und Forschung.
- ++ Supported in part by FOM, Vrije Universiteit Amsterdam and NWO.
- * Supported by KBN SPUB Nr 621/E -78/SPUB/P 3/209/94.
- ** Laboratory of CEA, Direction des Sciences de la Matière.

- a) Alexander von Humboldt fellow.
- b) Now at CERN, 1211 Genève 23, Switzerland.
- c) Now at Nikhef, 1009 DB Amsterdam, The Netherlands.
- d) Now at University of Padova, 35131 Padova, Italy.
- e) Now at MPI für Kernphysik, 69029 Heidelberg, Germany.
- f) Now at Université de Genève, 1211 Genève 4, Switzerland.
- g) Now at DPTA, CEA, Bruyères-le-Châtel, France.
- h) Now at Yale University, New Haven, 06511 CT, USA.
- i) Now at University of Mainz, 55099 Mainz, Germany.
- j) Now at University of Bonn, 53115 Bonn, Germany.
- k) Now at INFN-Instituto Superiore di Sanita, 00161 Roma, Italy.
- l) Now at Osaka University, 567 Osaka, Japan.
- m) Now at University of Michigan, Michigan, USA.
- n) Now at Stockholm University, 113 85 Stockholm, Sweden.
- o) Now at University of Erlangen-Nürnberg, 91058 Erlangen, Germany.
- p) Now at IKP2-KFA, 52428 Jülich, Germany.
- q) Now at University of Houston, 77204 TX, USA.
- r) Now at Dresden University, 01062 Dresden, Germany.
- s) Now at ESRF, 38043 Grenoble, France.
- t) Now at Tokyo Institute of Technology, Tokyo, Japan.
- u) Now at University of Freiburg, 79104 Freiburg, Germany.
- v) Now at Warsaw University of Technology, Warsaw, Poland.
- w) Now at Hamburg University, 22761 Hamburg, Germany.

1 Introduction

The structure function $F_2(x;Q^2)$ reflects the momentum distributions of the quarks in the nucleon. Because the proton and neutron have different contents of up and down quarks, a measurement of F_2^p and F_2^d , together with isospin symmetry, provides a constraint on the individual quark distributions; this is an important phenomenological input to the calculation of many strong interaction processes. In addition, the Q^2 dependence of F_2 can be used to test perturbative Quantum Chromodynamics (QCD), and to determine the strong coupling constant, α_s , and the momentum distribution of the gluons in the nucleon, $xG(x;Q^2)$. Measurements of $R(x;Q^2) = \frac{F_2^L}{F_2^T}$, the ratio of the longitudinally to transversely polarised virtualphoton absorption cross sections, can also be compared to QCD predictions computed from the measured values of F_2 and xG , thus providing an additional consistency check of

the theory.

In the deep inelastic scattering of charged leptons on nucleons, the differential cross section for one photon exchange can be written in terms of $F_2(x; Q^2)$ and $R(x; Q^2)$ as :

$$\frac{d^2 \sigma(x; Q^2; E)}{dx dQ^2} = \frac{4 \alpha^2}{Q^4} \frac{F_2(x; Q^2)}{x} \left(1 - \frac{y}{\frac{Q^2}{4E^2} + (1 - \frac{2m^2}{Q^2})} \frac{y^2 + Q^2 = E^2}{2(1 + R(x; Q^2))} \right); \quad (1)$$

where α is the fine structure constant, Q^2 the four momentum transfer squared, E the energy of the incident muon and m the muon mass. The Bjorken scaling variable, x , and y are defined as $x = Q^2/2M$ and $y = E^2/Q^2$, where E is the virtual photon energy in the laboratory frame and M is the proton mass¹. The one photon exchange cross section given by eq. (1) is obtained from the measured differential cross section by correcting for higher order electroweak effects.

When y is small enough, which is the case for most of the data presented here, the dependence of the one photon cross section on R is weak, as can be seen from eq. (1), and a measurement of the cross section is thus mainly a measurement of F_2 . In contrast, R can be obtained from the small differences in the cross section at given values of x and Q^2 but at different values of y , i.e. at different incident muon energies E .

In a recent article [1], we presented the structure functions of the proton and the deuteron, F_2^p and F_2^d , obtained from deep inelastic muon scattering at incident energies of 90, 120, 200 and 280 GeV. The data had been obtained between 1986 and 1989 using the large angle trigger of the experiment. This trigger recorded only events with scattering angles above 10 mrad and the accessible kinematic range did not allow a precise measurement of R . Hence the F_2^p and F_2^d measurements of ref. [1] were obtained using a parametrization [2] of earlier results on R . In the results presented here, the ranges of x and y covered have been extended downward by using data taken with a small angle trigger at 200 and 280 GeV in 1989. This has permitted the determination of R as well as F_2 .

2 The experiment and data selection

The experiment (NA 37) was performed at the M2 muon beam line of the CERN SPS. The proton and deuteron differential cross sections were measured simultaneously with two pairs of 3 m long targets placed alternately in the muon beam. In one pair the upstream target was liquid hydrogen and the downstream one liquid deuterium, while in the other pair the order was reversed. The spectrometer acceptance was substantially different for the upstream and downstream targets, thereby giving two separate measurements of the cross section for each material.

The integrated incident muon flux was continuously measured both by sampling the beam with a random trigger [3] and by sampling the counts recorded in two scintillator hodoscope planes used to determine the incident beam tracks [4]. In both cases the beam tracks present in these triggers were reconstructed off-line, in the same way as for scattered muon triggers, to determine the integrated usable flux.

Uncertainties on the incident and scattered muon momenta are important sources of systematic error. The forward spectrometer which measured the scattered muon momentum

¹This expression for the cross section, appropriate for fixed target experiments, can be expressed in relativistically invariant form by replacing $Q^2 = E^2$ with $4M^2 x^2 y^2 = Q^2$.

was calibrated to an accuracy of 0.2% using the reconstructed masses of J/ψ and K^0 mesons. The beam momentum spectrometer (BMS) was calibrated in dedicated runs by measuring the average incident muon momentum in a purpose built spectrometer [5]. The BMS was also calibrated relative to the forward spectrometer in a series of runs using precision silicon microstrip detectors. The results of the two BMS calibrations were averaged, leading to an accuracy of 0.2%. These calibrations are described in more detail in ref. [6].

The reader is referred to refs. [1, 7, 8, 9] for more details on the spectrometer, the large angle trigger and the analysis of the data obtained from this trigger. Properties specific to the small angle trigger are described below and in ref. [6].

The small angle trigger (see also ref. [7]) used three hodoscopes of 14 mm high, slightly overlapping, horizontal scintillator strips. Each hodoscope was vertically separated into two halves, above and below the muon beam. Coincidences between elements of each of the hodoscopes, which were about 5 m apart, selected particles whose trajectories were consistent with muons scattered from the targets. The narrow strips provided the necessary angular resolution and reduced the count rate per strip.

The small angle trigger collected events with scattering angles in the range $5^\circ < \theta < 25^\circ$ rad. Thus, this trigger detected events with smaller x and Q^2 than the large angle trigger ($x > 10^\circ$ rad). The small angle data cover the kinematic range $0.002 < x < 0.14$ and $0.5 < Q^2 < 25$ GeV 2 .

The following selections were applied in the analysis of the small angle trigger data (see table 1). The scattered muon momentum, p^0 , was required to be above a minimum value to suppress muons from hadron decays. Events with small (or y), where the spectrometer resolution was poor, were rejected. By requiring minimum scattering angles, θ_{min} , regions with rapidly varying acceptance were excluded. We imposed a maximum value of y in order to limit the contribution from higher order electroweak processes. In addition, the position of the reconstructed vertex was constrained to be within one of the targets. At each value of x , data in regions of Q^2 where the acceptance was less than 1%, or less than 25% of the maximum acceptance at that x , were removed. Regions close to the muon beam, whose efficiencies were difficult to describe, have been excluded from the analysis.

The number of events from the small angle trigger surviving these cuts was 0.54 million, while that from the large angle trigger was 1.82 million [1]. This is the full NMC data set covering the kinematic range $0.002 < x < 0.60$ and $0.5 < Q^2 < 75$ GeV 2 .

3 Data analysis

In order to measure the deep inelastic cross sections, one needs to take into account the effect of the spectrometer's resolution, which requires knowledge of the event distributions in the $(x; Q^2)$ plane and thus knowledge of the cross sections. In addition, the extraction of the structure functions from the measured cross sections requires the evaluation of the higher order electroweak contributions and thus *a priori* knowledge of the structure functions themselves. For these reasons, the structure functions were determined iteratively, using a Monte Carlo simulation of the experiment. Separate simulations were performed for each period of data taking, which enabled changes in the beam and the detector to be taken into account. All Monte Carlo events were processed through the same chain of reconstruction programs as the data, and weighted with the best knowledge of the total cross section. The accuracy of the Monte Carlo simulation was checked after the iterative process had converged by comparing, for each data period, the distributions of data and Monte Carlo events in variables not or only weakly related to x and Q^2 .

We discuss two iterative methods to compute F_2 and R . Method A had been used in our previous publications [4, 1], whereas method B was used in the present analysis.

3.1 M method A

In this method F_2 was calculated from all the data simultaneously. Parameterisations of F_2 and R were used, together with calculated higher order electroweak contributions, to determine cross sections which were used as the weights for the Monte Carlo events. The differences between the distributions of the accepted Monte Carlo events and the data led to a new parameterisation of F_2 , for input into the next iteration step. The parameterisation of R was taken from ref. [2] and kept fixed in the iteration. Convergence was considered reached when the values of F_2 changed by less than 0.2%, in practice after two iterations.

In this determination of F_2 it was assumed that the parameterisation of R , valid for $x > 0.015$ [2], could be extrapolated to small values of x ; the validity of this assumption is discussed in section 6. The main advantage of method A is that it uses the information on F_2 over the full kinematic range at each step of the iterative process.

3.2 M method B

In this method, used in the present publication, the iterative procedure was split in two [9], which facilitates the extraction of R as well as F_2 from the data.

First, the scattering cross sections were extracted separately for each data set taken at a given energy and target position with a given trigger. For each such data set, the cross sections were parameterised using the product of a 10-parameter function [9] and the Monte Carlo cross section and used as the weights for the Monte Carlo events. In this iterative procedure the cross sections were determined but were not corrected for higher order electroweak processes. Convergence to better than 0.2% was reached after typically three iterations.

In the second step all the extracted cross sections were corrected for higher order electroweak processes and used simultaneously to determine F_2 and R . Again this was done iteratively, and typically convergence was reached after two iterations. In this procedure, F_2^p and F_2^d were parameterised using the 15-parameter function of ref. [1]; the parameterisation of R is discussed in section 4.

The individual extraction of the cross sections for each data set in the first step of method B leads to a different sensitivity to uncertainties in the acceptance to that of method A. Thus a comparison of the results from the two methods provides information on the overall acceptance uncertainty as well as on the reliability of the methods used to extract F_2 and R . The results of the two methods were found to agree to a fraction of a percent, except at the largest x , if the values of R in method B were taken to be the same as in method A.

3.3 Relative normalisations

The cross section measurements are affected by normalisation uncertainties which are of the order of 2% [1]. To estimate possible normalisation shifts, we have fitted simultaneously the proton and deuteron structure functions F_2^p and F_2^d from the present analysis together with those from BCDMS [10] and SLAC [11], again using the 15-parameter function of ref. [1].

For the NMC data there were six normalisation parameters (one per energy and trigger), and the same normalisation parameters were used for the proton and deuteron data owing to the simultaneous data taking; the other four data sets each had one normalisation parameter. The 2 of the t included the shifts, weighted according to the quoted normalisation uncertainties of the experiments. In order to reduce the sensitivity of the fitted parameters to systematic uncertainties and to the value of R , we excluded data at small and large y from the t . The resulting shifts are given in table 2; they were determined using data in the range $0.2 < y < 0.5$. We checked that they do not significantly depend on the particular y range used. The shifts are all compatible with the normalisation uncertainties quoted by the experiments; they are close to those obtained in ref. [1]. For the results presented in the rest of this paper the normalisation shifts of table 2 have been applied.

4 The extraction of F_2 and R

Where at least two cross section measurements are available at a given x and Q^2 for different incident muon energies, it is possible to determine the function $R(x;Q^2)$ from the weak dependence of the cross section on y , as can be seen from eq. (1). Data points at small y are mainly sensitive to F_2 , while at large y they are also sensitive to R . The inclusion in the present analysis of the small-angle trigger data, which have smaller average values of y and are thus less sensitive to R than the large angle trigger data, allows in principle a simultaneous determination of F_2 and R . In practice, the extraction of R was limited as follows:

The sensitivity of our data to R is substantial only at small x (see figure 1). For $x > 0.12$ almost all our data are at $y < 0.40$ and there is little sensitivity to R . Thus the simultaneous determination of F_2 and R was not possible over the full kinematic range of our measurement.

The study of systematic uncertainties on R showed that the present data do not allow a measurement of both its x and Q^2 dependence.

We have extracted the average R for the proton and the deuteron. This is justified by the NMC results on the cross section ratio F_2^d/F_2^p [12], with more events and smaller systematic errors than the data described here, which show that in the kinematic range $0.002 < x < 0.40$, $R^d - R^p$ is compatible with zero to within 0.02 (see also refs.[2, 13]).

As a consequence, we have chosen the following procedure for the extraction of F_2 and R . For $x < 0.12$, we determined in each bin of x one Q^2 averaged value of R , together with the values of $F_2^p(x;Q^2)$ and $F_2^d(x;Q^2)$. In the lowest x bin, $x = 0.0045$, where our data span a very small interval, the determination of R relies on the extrapolation of F_2^p and F_2^d from neighbouring bins at larger x . At $x > 0.12$, where R is known from other measurements, we used the R parametrisation given in ref. [2] in the determination of the structure functions, F_2 .²

To summarize, the final results of this analysis, given below in sections 5 and 6, were obtained using the method described in this section and in sections 3.2 and 3.3.

²We remark that most of the 139 measurements of R used to obtain the parametrisation in ref. [2] are for $x = 0.10$. In contrast, for $x < 0.10$ where our data are most sensitive to R , the remaining 5 measurements of R have total errors of typically 40%.

4.1 Systematic uncertainties on F_2

The systematic uncertainties on the large angle trigger data have been discussed in ref. [1]. Here, we discuss only those for the small angle trigger data.

As in ref. [1] the uncertainty in the determination of the spectrometer acceptance was studied by comparing the structure functions determined separately from the upstream and the downstream targets, for which the spectrometer has largely different acceptances. This uncertainty was also studied by comparing the structure function results obtained from methods A and B described above. These studies led to an estimated contribution to the systematic error on F_2 usually in the range 0.5–2%, reaching 4% at the edge of the kinematic domain in x and Q^2 . The spectrometers' calibration uncertainties of 0.2% discussed in section 2 contributed at most 1.5% to the systematic uncertainty on F_2 .

The effect of hadronic and electromagnetic showers on the reconstruction efficiency was determined from a simulation of the final state, following the method described in refs. [4, 6]. For the small angle trigger the loss of efficiency due to these showers was much larger than for the large angle trigger. The resulting inefficiency was found to be independent of Q^2 and thus was parameterised as a function of x only. At the smallest x ($x = 0.0045$) it amounts to about 20% decreasing linearly with $\ln x$ to zero at $x = 0.1$. The consequent systematic error on F_2 was estimated to be 1.5 to 4%.

The higher order electroweak contributions to the cross sections and their uncertainties were calculated as in ref. [1] using the method of ref. [14]. These contributions were at most 20% (at $x = 0.005$ and $y = 0.75$) and generally much smaller. The consequent systematic errors on F_2 are typically less than 1%, but can reach 2% at large y . They arise predominantly from the uncertainties in R , in the proton form factor and in the suppression of the quasi-elastic scattering on the deuteron. The uncertainty in R contributes both here and through the calculation of the one photon exchange cross section.

The normalisation uncertainty of the data at each incident energy, relative to the fitted function describing F_2 used in the iteration, is estimated to be 2% (see also section 3.3 and table 2). This is included in the 2.5% total normalisation uncertainty of the combined data. Because the hydrogen and deuterium targets were simultaneously exposed to the beam, the uncertainty on the relative normalisation of F_2^p and F_2^d is negligible.

The total systematic uncertainties on F_2 , obtained by adding in quadrature all the above contributions apart from the normalisation uncertainty, range from 1% to 5%, with a median value of 2%.

4.2 Systematic uncertainties on R

The largest contribution to the systematic error on R stems from the 2% uncertainties in the relative normalisations of the six data sets. It was estimated by varying the normalisation of each data set in turn and recalculating R and F_2 . The quadratic sum of the resulting variations in R was taken as one contribution to the systematic uncertainty.

The other sources of uncertainty are the same as those for F_2 , discussed above. These are the uncertainties in the incident and scattered muon momenta, the higher order electroweak contributions, the acceptance and the reconstruction losses; the last three were assumed to be fully correlated between data sets. The contributions of these uncertainties to the systematic error on R were determined by recalculating R with the cross sections shifted according to each uncertainty in turn.

The individual contributions to the systematic error on R were added in quadrature giving total uncertainties ranging from 0.11 at $x = 0.0045$ down to 0.07 at $x = 0.11$; the

uncertainties are largely correlated.

4.3 Alternative extractions of R

The extraction of R described above used parametrizations of F_2^P and F_2^d over the full kinematic domain of the measurement. This has the advantage of being less sensitive to Q^2 dependent and data set dependent systematic uncertainties of the cross sections, but introduces correlations between the statistical errors on R in neighbouring x bins.

In order to cross check our standard method of calculating R, we performed two other extractions whose results are shown in figure 2. Both checks used the one photon exchange cross sections obtained in method B (section 3.2) adjusted by the normalization shifts of table 2. The corrections for higher order electroweak effects were calculated with the SLAC parametrization for R, but without any iteration.

The first check, labelled check 1 in figure 2, evaluated R and F_2 at each x bin independently, using all the measured cross sections in that bin. We fitted an average value of R and a parametrization of F_2^d to the one photon exchange cross sections for each x bin in the range $0.006 < x < 0.12$ in turn. The parametrization for F_2^d which we used, and which we checked to be sufficiently flexible to describe our data, was

$$\ln F_2^d(x_i; Q^2) = (a_i + b_i \ln(Q^2)) + \ln(1 + c_i/Q^2);$$

while F_2^P was obtained by dividing the F_2^d parametrization by our measured ratio F_2^d/F_2^P [12].

The second check (check 2) followed the traditional "method, as e.g. in the SLAC analysis [2], which uses the individual $(x; Q^2)$ bins one at a time. The ratio R ($= L/T$) was obtained from the variation of the cross section as a function of y within each bin, using the cross sections expressed in a form proportional to $T + "L"$, where " L " $\propto 1/(y^2 + Q^2/E^2) = 2(1 - y/Q^2 = 4E^2)$. A linear fit to the cross section as a function of " y " yielded a determination of R in each $(x; Q^2)$ bin in which measurements from at least three energies are available.

As can be seen in figure 2, the results of the two checks agree well with those of the present analysis, given their different sensitivities to systematic errors.

5 Results for F_2

The results obtained for the structure functions F_2^P and F_2^d for all energies and triggers are shown in figures 3 and 4 as a function of Q^2 for fixed values of $x < 0.12$. They were obtained for all six data sets using method B (the data of ref. [1] were re-evaluated). In these figures, the error bars represent the quadratic sum of the statistical and systematic errors. The small angle data extend the measured x domain downwards to $x = 0.0045$; they also fill gaps in the Q^2 range covered by the large angle trigger data. Within the quoted uncertainties, there is good agreement between all data sets. It may be noted that if $R = 0$ was used in the analysis, the Q^2 dependence of the F_2 data in the small x bins became noticeably less smooth.

The values of $F_2^P(x; Q^2)$ and $F_2^d(x; Q^2)$ and the various contributions to the systematic errors are given in tables 3 (a{d}) and 4 (a{d}); the scattering cross sections, $d^2 \text{m}^{\text{eas}} = dx dQ^2$, not corrected for higher order electroweak effects, are also given. In these tables, the results from the two triggers in the data taken at 200 and 280 GeV were averaged.

In figures 5 and 6 we show the measured F_2^P and F_2^d averaged over the four energies. The corresponding values are given in tables 5 and 6. We also give in these tables values of F_2^P

and F_2^d determined if we use the SLAC parametrisation of R (R_{1990}); the difference becomes sizeable at small x .

Our results are in good agreement with those of SLAC [11] and BCDM S [10] as is shown in figure 7 for the deuteron. Recently, new results extending down to $x = 0.0008$ have become available from the fixed target muon scattering experiment E 665 at Fermilab [15]. In figure 8 our data on F_2^p and F_2^d are compared with the E 665 results for $0.004 < x < 0.04$. The agreement is generally good, except perhaps around $x = 0.01$ for F_2^d . Note that E 665 uses R_{1990} while we use in this small x region our own measurement for R . However, this does not influence the comparison since the E 665 data are not very sensitive to R (because they cover the small x region).

In figure 9 we present a comparison of the NMC data with the results obtained by the H1 [16] and ZEUS [17] collaborations at HERA from their 1994 data. These new HERA results agree much better with the NMC data than the earlier ones and the gap in Q^2 between the HERA and NMC data has become smaller (see e.g. ref.[1]).

6 Results for R

In this section, we present the results on R , obtained from the combined proton and deuteron data, in the range $0.002 < x < 0.12$. Figure 10(a) shows these results for R as a function of x at an average Q^2 ranging from $4Q^2 i = 1.4$ to 20.6 GeV 2 for the different x -bins. The corresponding values are given in table 7. In the figure the error bars indicate the quadratic sum of statistical and systematic uncertainties. The systematic errors are 1.5 to 3 times larger than the statistical ones; they are dominated by the normalisation uncertainty and are thus largely correlated.

In figure 10(a), we also compare the present results for R with the parametrisation of ref. [2] used in previous measurements of F_2 , and with a QCD prediction. Within the largely correlated systematic errors, the agreement with the parametrisation is good, even at small x where the parametrisation is an extrapolation of previous measurements.

The QCD prediction for R was calculated as

$$R(x;Q^2) = \frac{F_L(x;Q^2) + \frac{4M^2x^2}{Q^2} F_2(x;Q^2)}{F_2(x;Q^2) - F_L(x;Q^2)}; \quad (2)$$

using the formula of ref. [18] for the longitudinal structure function F_L in next to leading order QCD,

$$F_L(x;Q^2) = \frac{s(Q^2)}{2} x^2 \int_x^{Z^{-1}} \frac{dw}{w^3} \left[\frac{8}{3} F_2^{SI}(w;Q^2) + \frac{40}{9} \left(1 - \frac{x}{w}\right) w G(w;Q^2) \right]; \quad (3)$$

where F_2^{SI} is the singlet quark and xG the gluon momentum distribution. In evaluating this expression, we have taken the F_2^d parametrisation from ref. [1] for F_2^{SI} , and used the gluon distribution from a QCD analysis of BCDM S, NMC and H1 data [16]; as in this analysis, we set $s(50\text{GeV}^2) = 0.180$ [19]. The agreement is good, even at small Q^2 and x where the validity of the Altarelli-Martinelli relation might be questioned, and the uncertainty on the gluon distribution is large.

In figure 10(b) we compare the present R measurement to other results obtained at comparable x and Q^2 by BCDM S [10, 20] and CDSHW [21]. Good agreement is observed; the present results are lower but the difference is within the largely correlated uncertainties of the experiments. The NMC results improve the knowledge of R for $x < 0.1$ considerably.

In figures 10 (b) and 11, the R measurements shown have been obtained from very different target materials. There is no evidence for a significant A dependence of R , consistent with perturbative QCD expectations. Similar conclusions were reached from measurements of differences between R for various nuclei [13, 22, 23, 24].

In figure 11, we compare in Q^2 bins the present results with others, mostly obtained at SLAC [2, 22, 23] at larger x . In these plots, no significant x -dependence is observed for Q^2 between 1.5 and 20 GeV 2 . Thus one may conclude that the x dependence observed in figure 10 (b) is a reflection of the variation of the average Q^2 with x .

7 Summary

We have extracted F_2^p , F_2^d and R from measurements of inclusive deep inelastic muon scattering on the proton and the deuteron at 90, 120, 200 and 280 GeV. The results for F_2^p and F_2^d cover the kinematic range $0.002 < x < 0.60$ and $0.5 < Q^2 < 75$ GeV 2 , with high statistical accuracy and with systematic uncertainties between 1% and 5%. The data are in good agreement with the earlier high statistics results from SLAC and BCDMS, as well as with more recent data at small x from the Fermilab E665 experiment and from H1 and ZEUS at HERA. Results for R cover the kinematic range $0.002 < x < 0.12$ and $1.0 < Q^2 < 25$ GeV 2 , extending its knowledge to small values of x . They are in agreement with earlier measurements as well as with expectations from perturbative QCD.

References

- [1] NMC, M. Amendo et al., Phys. Lett. B 364 (1995) 107,
and preprint CERN-PPE/95-138 for the tables.
- [2] L.W. Whitlow et al., Phys. Lett. B 250 (1990) 193.
- [3] R.P. Mount, Nucl. Instrum. Methods 187 (1981) 401.
- [4] NMC, P. Amadruz et al., Phys. Lett. B 295 (1992) 159.
- [5] M. Amendo, Ph.D. Thesis, Princeton University (1992).
- [6] A. Dyring, Ph.D. Thesis, Uppsala University (1995).
- [7] NMC, P. Amadruz et al., Nucl. Phys. B 371 (1992) 3.
- [8] M. van der Heijden, Ph.D. Thesis, University of Amsterdam (1991);
I.G. Bird, Ph.D. Thesis, Free University, Amsterdam (1992);
A. Brüll, Ph.D. Thesis, Freiburg University (1992) (in German);
T. Granier, Ph.D. Thesis, Université Pierre et Marie Curie, Paris (1994) (in French).
- [9] P. Björkholm, Ph.D. Thesis, Uppsala University (1995).
- [10] BCDMS Collab., A.C. Benvenutti et al., Phys. Lett. B 233 (1989) 485;
BCDMS Collab., A.C. Benvenutti et al., Phys. Lett. B 237 (1990) 592.

- [11] L.W .W hitlow et al, Phys.Lett B 282 (1992) 475.
- [12] NM C , M .A meodo et al, subm . to Nucl.Phys.B ,
- [13] NM C , P .Am audruz et al, Phys. Lett.B 294 (1992) 120.
- [14] A A .A khundov et al, Sov.J.Nucl.Phys. 26 (1977) 660; 44 (1986) 988;
JINR-D ubna preprints E2-10147 (1976), E2-10205 (1976), E2-86-104 (1986);
D .Bardin and N .Shum eiko, Sov.J Nucl.Phys. 29 (1979) 499.
- [15] E 665 Collab., preprint Fermilab-Pub-95/396-E , subm . to Phys. Rev.D ;
A .V .K otwal, Ph.D .T hesis, H arvard U niversity (1995).
- [16] H 1 Collab., S .A id et al, Nucl.Phys.B 470 (1996) 3.
- [17] ZEUS Collab., M .D errick et al, preprint DESY 96-076, subm . to Z .Phys.C .
- [18] G .A ltarelli and G .M artinelli, Phys. Lett.B 76 (1978) 89.
- [19] M .V irochaux and A .M ilszta jn, Phys. Lett.B 274 (1992) 221.
- [20] BCDMS Collab., A .C .B envenutiet al., Phys. Lett.B 195 (1987) 91.
- [21] CDHSW Collab., P .B erge et al, Z .Phys.C 49 (1991) 187.
- [22] E 140 Collab., S .D asu et al, Phys. Rev. Lett. 61 (1988) 1061;
E 140 Collab., S .D asu et al, Phys. Rev.D 49 (1994) 5641.
- [23] E 140X Collab., L H .Tao et al, Z .Phys.C 70 (1996) 387.
- [24] NM C , M .A meodo et al, subm . to NuclPhys. B .

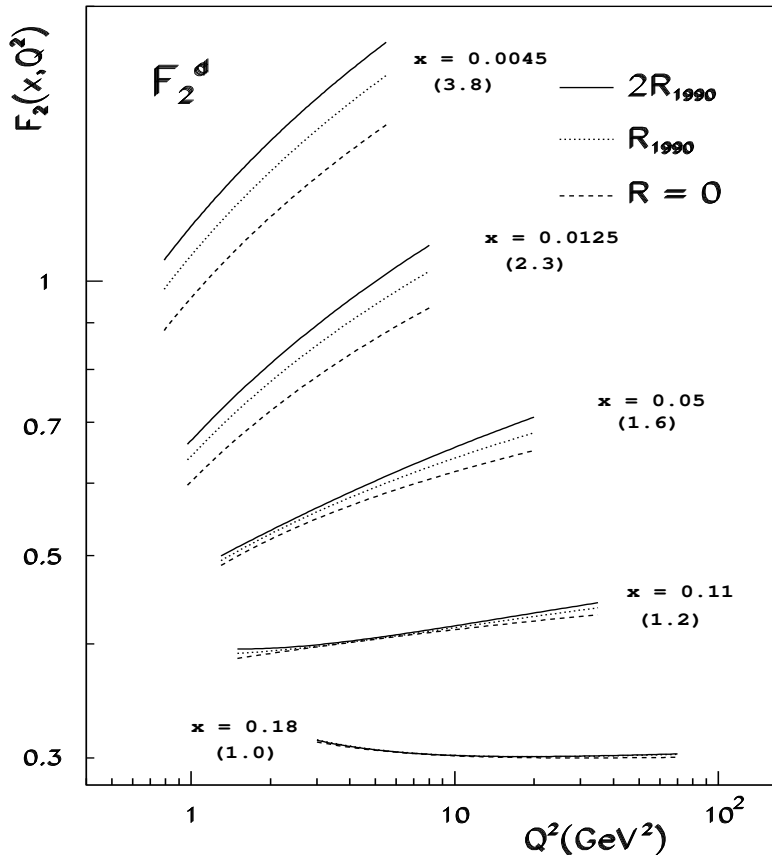


Figure 1: The sensitivity of the measured structure function F_2^d to the assumed value of R . This is illustrated for x bins. The lines indicate the results of fits to F_2^d computed assuming R to be given by the R_{1990} parametrization of ref. [2] (dotted), twice that parametrization (solid), or zero (dashed) for x bins, with F_2 scaled by the numbers in brackets.

Incident energy (GeV)	p_m^0 in (GeV)	m_{in} (GeV)	m_{up} (m rad)	m_{down} (m rad)	Y_m in	Y_m ax	N_p (10^3)	N_d (10^3)
200	35	15	6-6.5	6.5-7	{	0.8	78	162
280	40	30	6-7	6-7.5	0.2	0.8	97	207

Table 1: Cuts applied to the small angle trigger data, as explained in the text. Different values of m_{in} were used for the upstream and downstream targets and for different data taking periods. N_p and N_d are the total number of events for protons and deuterons, respectively, after applying all cuts.

Data set	P roton	D euteron
	B oth	
SLAC	{0.4%	+ 0.9%
BCDM S	{1.8%	{0.7%
NMC 90 GeV		{2.7%
NMC 120 GeV		+ 1.1%
NMC 200 GeV T1		+ 1.1%
NMC 280 GeV T1		+ 1.7%
NMC 200 GeV T2		{2.9%
NMC 280 GeV T2		+ 2.0%

Table 2: Normalisation changes for the different data sets. All numbers were obtained from the fits described in section 3.3. The normalisation uncertainties quoted by the experiments are respectively 2%, 3% and 2% for SLAC, BCDM S and NMC.

x	$hQ^2 i$ (GeV ²)	range of y	R	statistical error	systematic error
0.0045	1.38	0.63-0.74	0.537	0.067	0.110
0.0080	1.31	0.49-0.77	0.337	0.044	0.112
0.0125	2.20	0.40-0.75	0.246	0.037	0.110
0.0175	3.12	0.28-0.73	0.190	0.036	0.109
0.025	4.5	0.20-0.74	0.099	0.032	0.090
0.035	7.0	0.20-0.73	0.108	0.030	0.080
0.050	10.2	0.17-0.69	0.117	0.030	0.079
0.070	14.1	0.12-0.69	0.113	0.049	0.076
0.090	16.9	0.10-0.57	0.096	0.036	0.079
0.110	20.6	0.10-0.60	0.043	0.041	0.067

Table 7: Results for R as a function of x; $hQ^2 i$ is the mean value of Q^2 at which R was determined. The range of y covered by the data is also given.

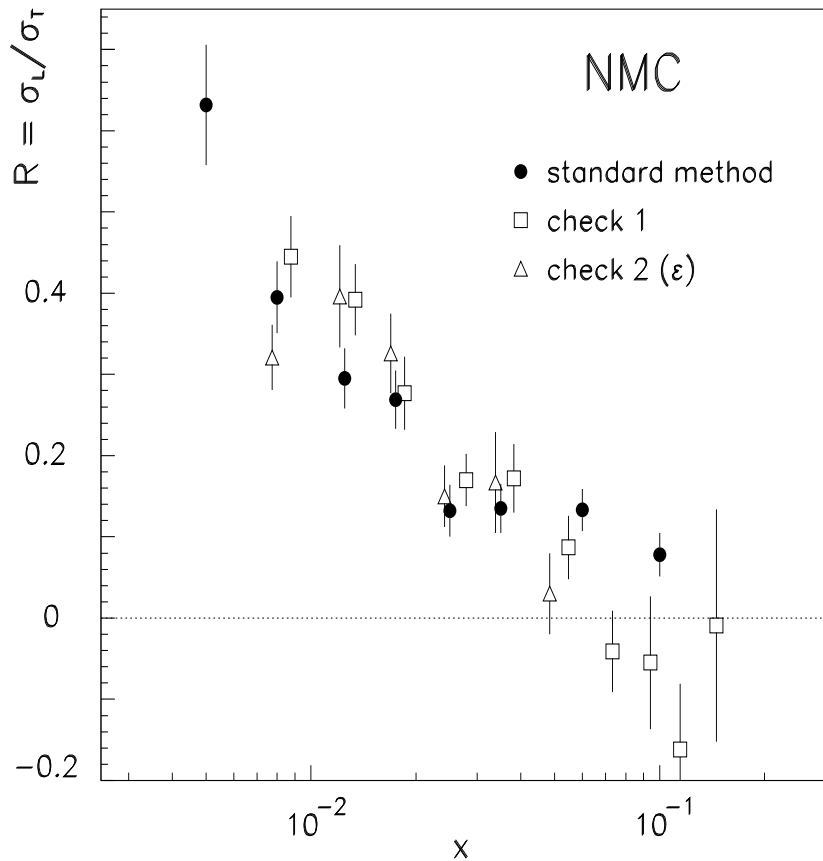


Figure 2: The standard NMC method for calculating R (filled circles) compared to two alternative extractions described in the text, per x bin (open squares) or per $(x; Q^2)$ bin (open triangles). Only statistical errors are shown. The three extractions are compared before any iteration is performed; in particular, the results shown for the standard method are not the final ones (these are shown in figs. 10 and 11).

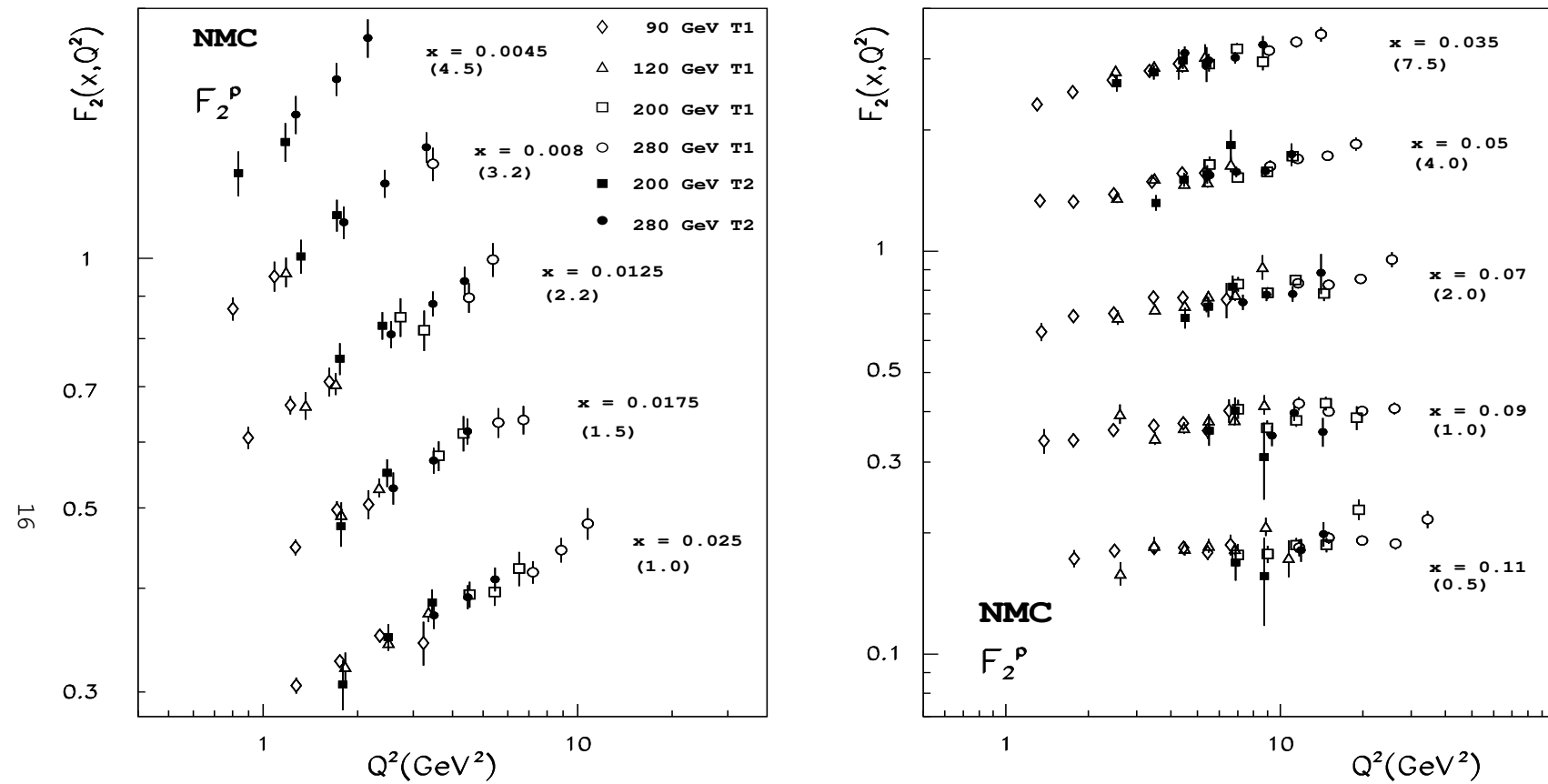


Figure 3: The structure function $F_2^P(x; Q^2)$ versus Q^2 in bins of x . The six data sets correspond to four different incident energies and two triggers. The new small angle trigger data are shown as filled symbols; bins of x where no small angle data exist are not shown. The data in each x bin have been scaled by the factors indicated in brackets. The error bars represent the quadratic sum of systematic and statistical errors. The normalisation uncertainties are not included.

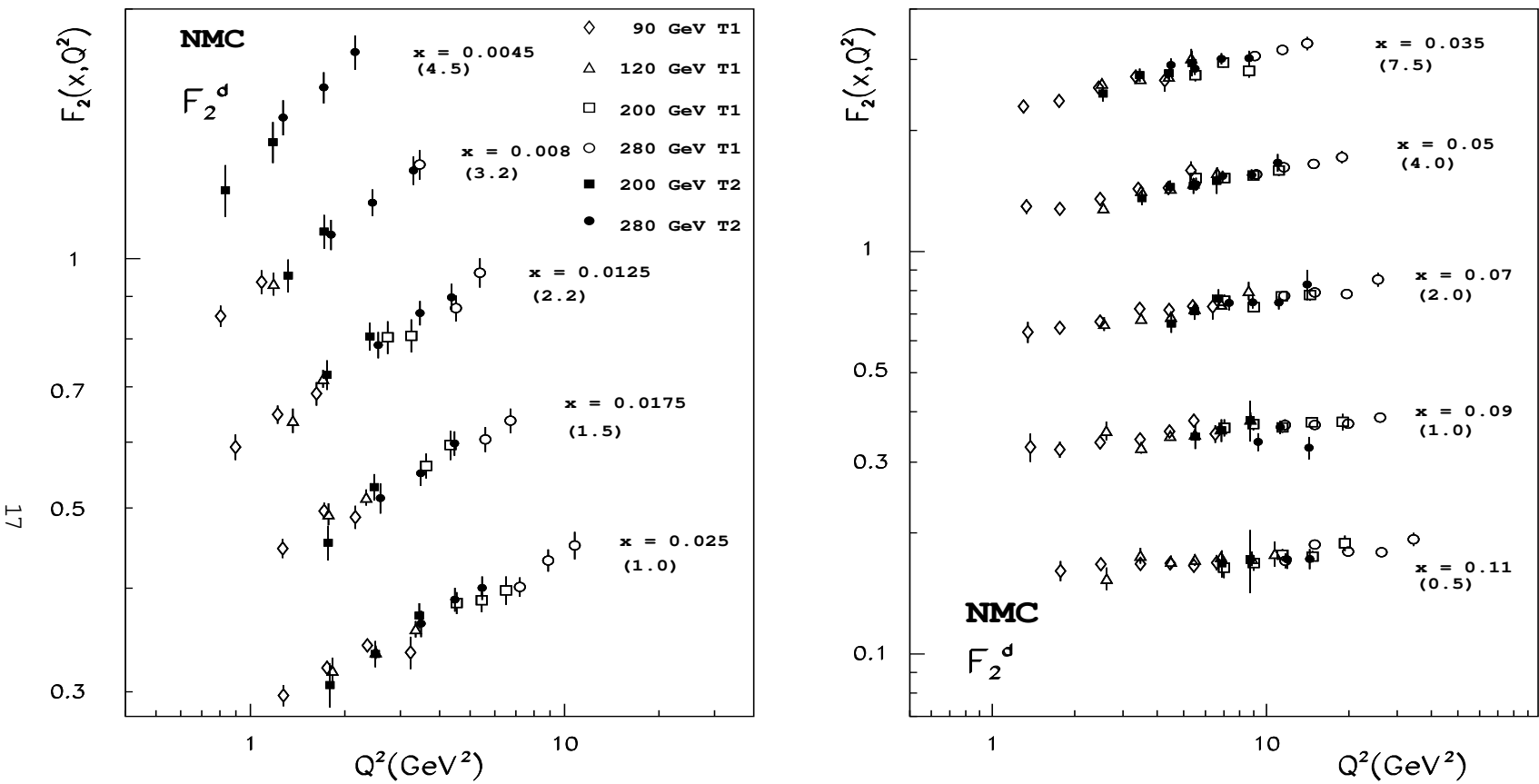


Figure 4: The structure function $F_2^d(x; Q^2)$ versus Q^2 in bins of x . The six data sets correspond to four different incident energies and two triggers. The new small angle trigger data are shown as filled symbols; bins of x where no small angle data exist are not shown. The data in each x bin have been scaled by the factors indicated in brackets. The error bars represent the quadratic sum of systematic and statistical errors. The normalisation uncertainties are not included.

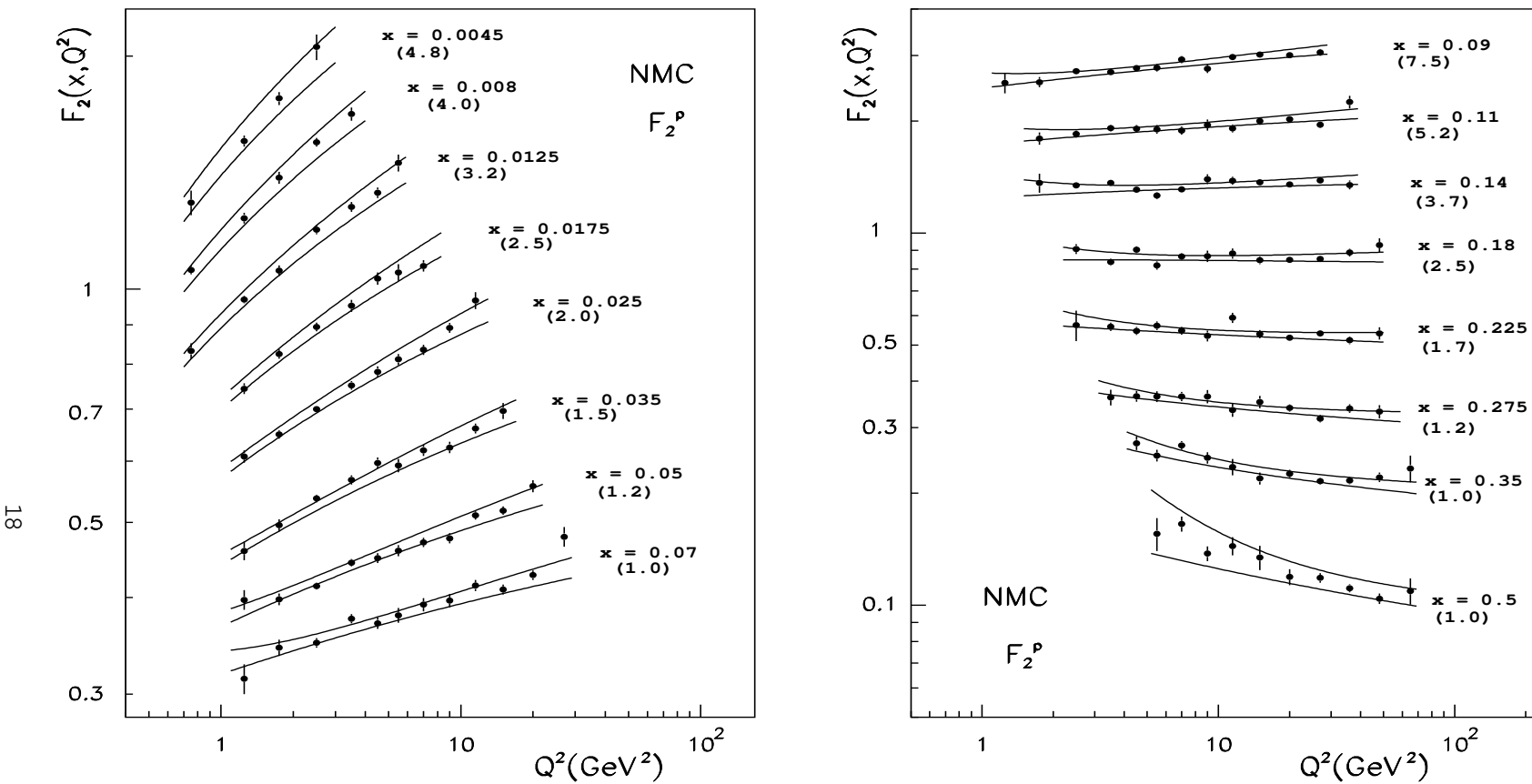


Figure 5: The structure function $F_2^p(x; Q^2)$ versus Q^2 in bins of x . The corresponding values are given in table 5. The six data sets of g. 3 have been averaged. The data in each x bin have been scaled by the factors indicated in brackets. The error bars represent the statistical errors; the total systematic uncertainties, apart from the 2.5% normalisation uncertainty, are indicated by the bands.

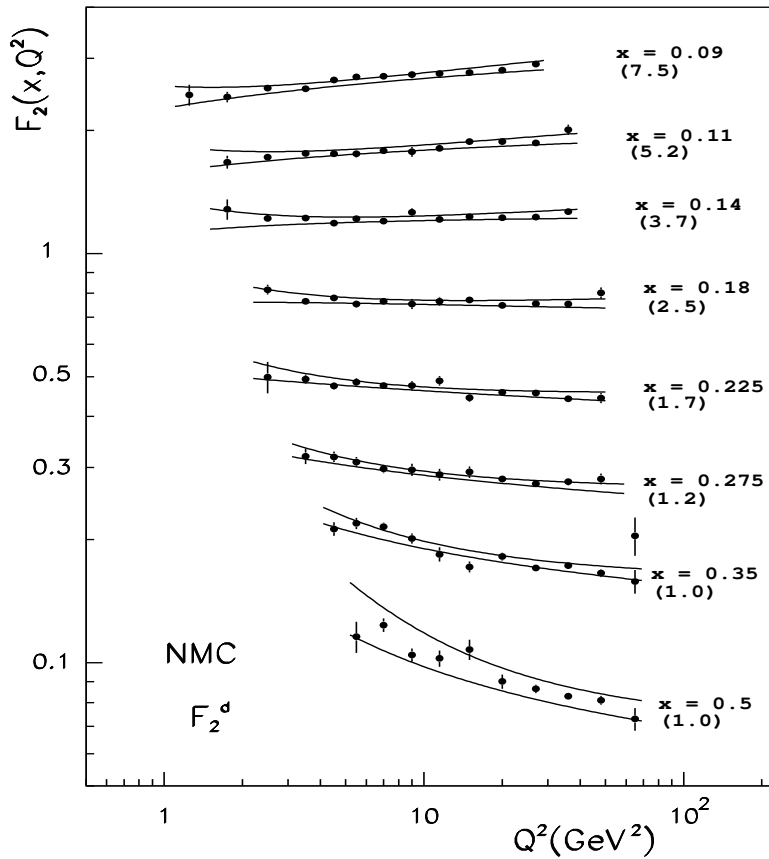
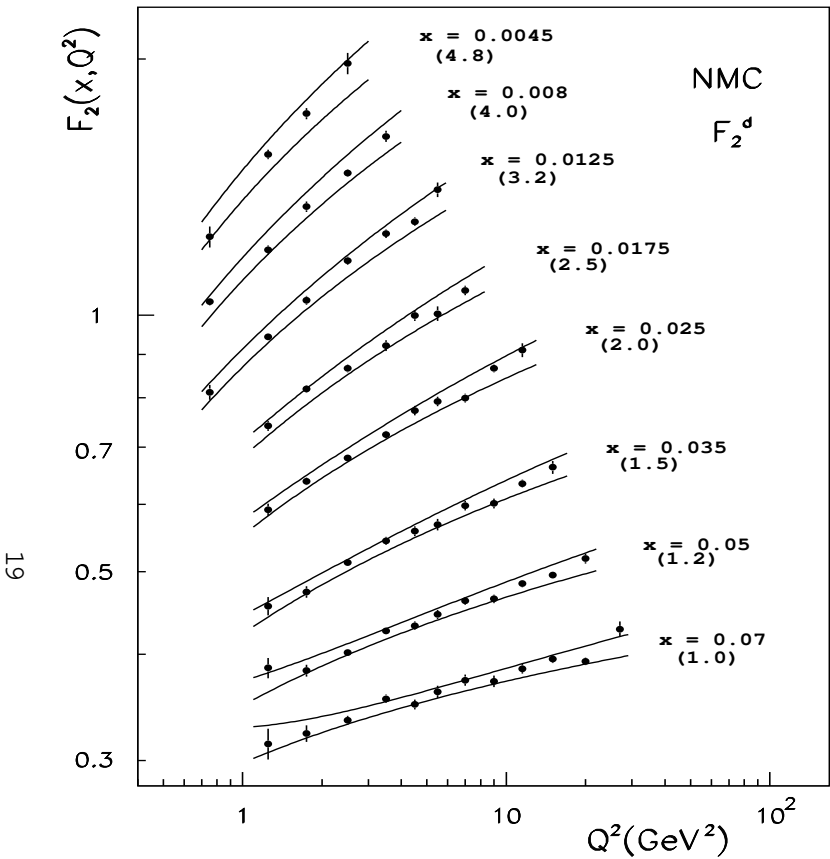


Figure 6: The structure function $F_2^d(x; Q^2)$ versus Q^2 in bins of x . The corresponding values are given in table 6. The six data sets of g. 4 have been averaged. The data in each x bin have been scaled by the factors indicated in brackets. The error bars represent the statistical errors; the total systematic uncertainties, apart from the 2.5% normalisation uncertainty, are indicated by the bands.

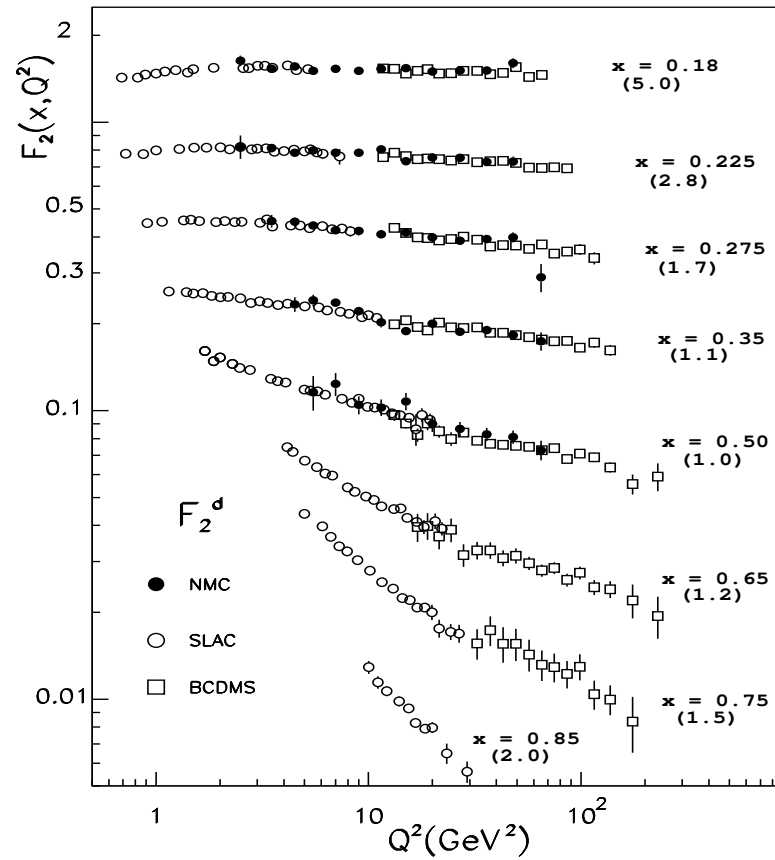
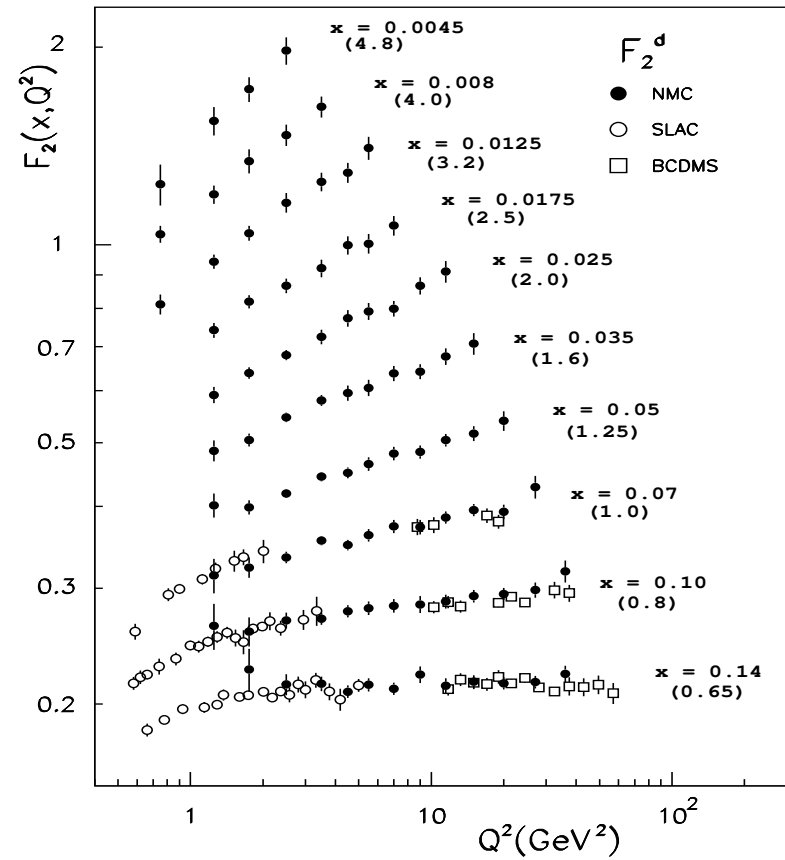


Figure 7: The present results for F_2^d (filled circles) compared to those of BCDMS [10] (open squares) and SLAC [11] (open circles). The data have been adjusted by the normalisation shifts of table 2, and the BCDMS data have been corrected by their calibration uncertainty, as in ref. [1]. At $x = 0.50$ the BCDMS and SLAC data have been interpolated. The data in each x bin have been scaled by the factors indicated in brackets. The error bars represent the total errors, apart from normalisation uncertainties.

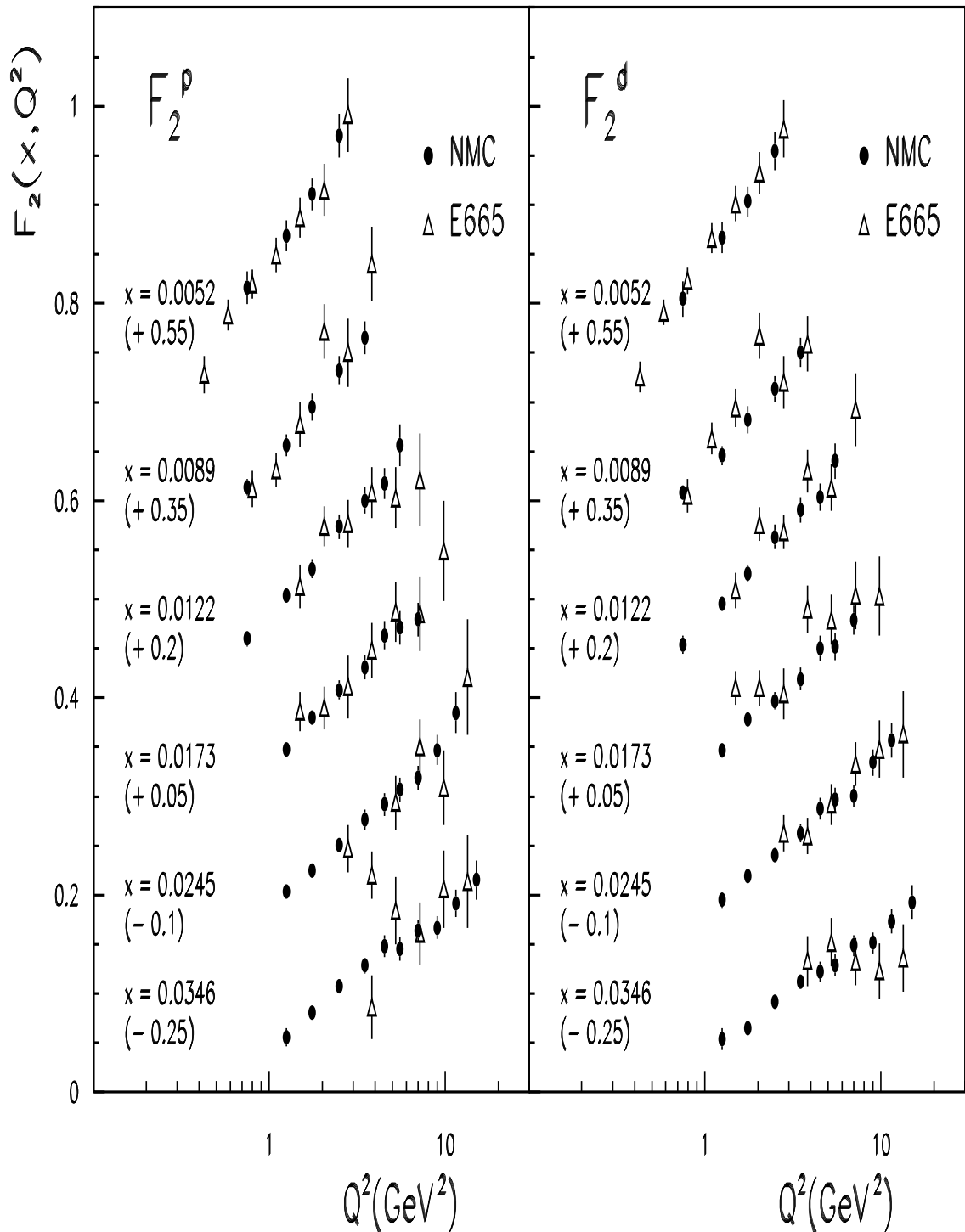


Figure 8: The structure function F_2^P and F_2^d from the present measurement (filled circles) compared to those of the E665 experiment at Fermilab [15] (open triangles), in the range $0.004 < x < 0.04$. The NMC data have been interpolated to the E665 x bins. The data in

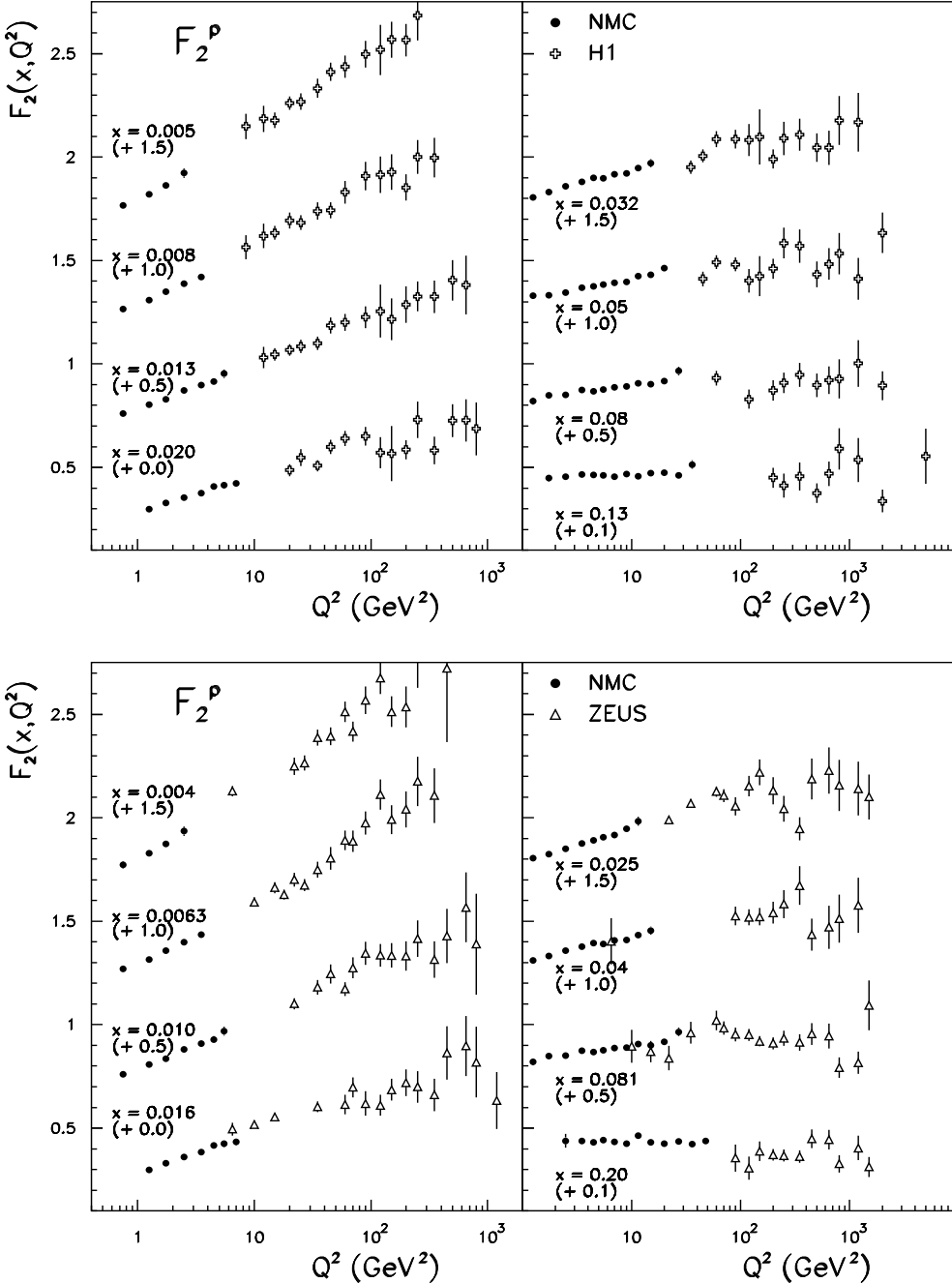


Figure 9: The structure function F_2^P from the present measurement (filled circles) compared to those of the DESY experiments H1 [16] (top, open crosses) and ZEUS [17] (bottom, open triangles), in the range $0.004 < x < 0.20$. The NMC data have been interpolated to the H1 and ZEUS x bins. The data in each x bin have been offset by the amounts indicated in brackets. The errorbars, wherever visible, represent the total errors, apart from normalisation uncertainties.

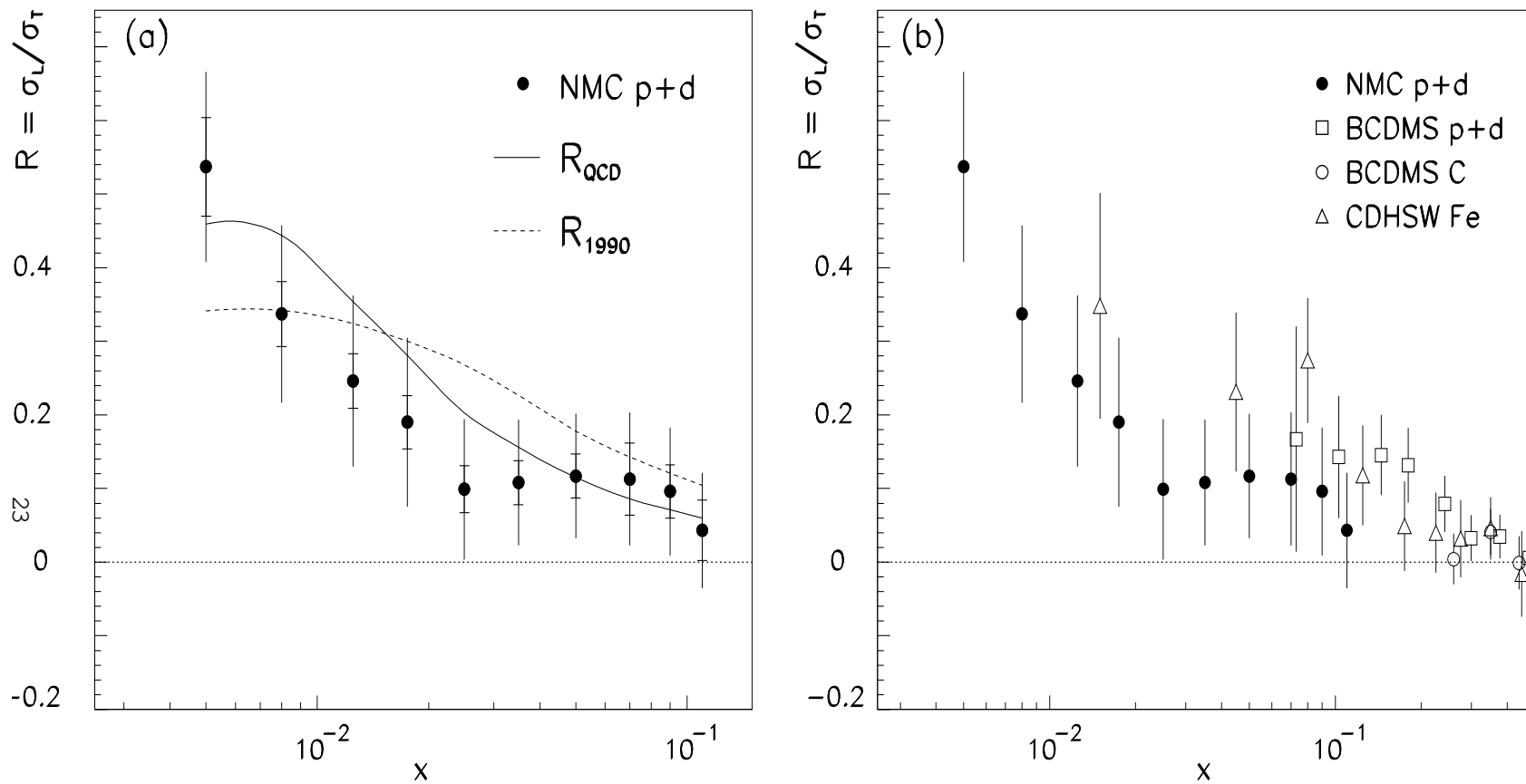


Figure 10: (a) The ratio R measured in this experiment, averaged for the proton and the deuteron. The outer error bars represent the quadratic sum of the statistical and systematic uncertainties; the inner bars indicate the statistical errors. The dashed line represents the R parametrisation from ref. [2] at the average Q^2 of each x bin. The solid line indicates a QCD calculation described in the text. (b) The ratio R measured in this experiment (filled circles), compared to previous results at comparable x and Q^2 obtained by BCDMS [10, 20] (open squares and circles) and by CDHSW [21] (open triangles). The error bars represent the total errors.

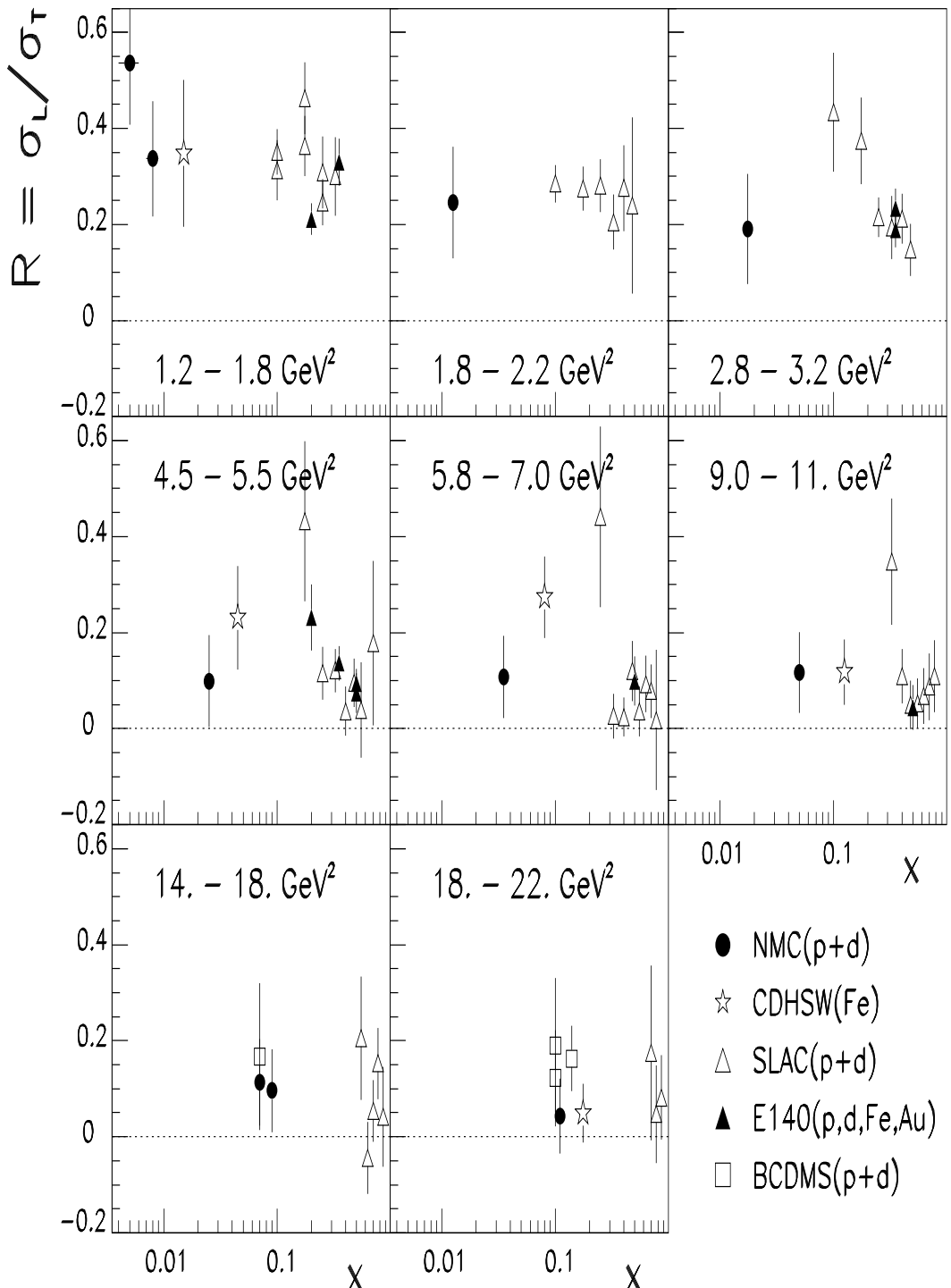


Figure 11: The x dependence of the ratio R in bins of Q^2 as measured in this (NMC, filled circles) and previous experiments. These are mainly the SLAC hydrogen and deuterium scattering experiments [2] (open triangles) and the SLAC E140 experiments [22, 23] (filled triangles); also shown are results from CDHSW [21] (open stars) and BCDMS [10] (open squares). The error bars represent the total errors.

x	Q^2 (GeV ²)	y	$d^2_{p} \frac{m}{p} \text{eas} = dx dQ^2$ (b / GeV ²)	E [%]	E ⁰ [%]	A C [%]	R C [%]	R E [%]	R	F ^P ₂	F ^{stat} ₂	F ^{syst} ₂
0.0087	1.18	0.626	3.938e-06	0.5	0.0	2.1	1.6	0.6	0.337	0.2987	0.0090	0.0082
0.0117	1.37	0.540	2.400e-06	0.7	-0.2	1.6	1.1	0.4	0.246	0.3030	0.0097	0.0062
0.0129	1.70	0.604	1.410e-06	0.5	0.0	1.5	1.2	0.5	0.246	0.3200	0.0071	0.0066
0.0172	1.77	0.472	1.109e-06	0.7	-0.2	1.2	0.7	0.4	0.190	0.3274	0.0100	0.0052
0.0178	2.34	0.599	6.064e-07	0.6	0.0	1.1	1.0	0.5	0.190	0.3519	0.0072	0.0057
0.0241	1.82	0.351	8.159e-07	0.9	-0.4	0.7	0.3	0.3	0.099	0.3219	0.0122	0.0042
0.0245	2.50	0.471	4.142e-07	0.7	-0.2	0.8	0.5	0.4	0.099	0.3440	0.0054	0.0043
0.0260	3.36	0.590	2.170e-07	0.6	0.0	1.0	1.2	0.5	0.099	0.3732	0.0077	0.0064
0.0348	2.51	0.332	3.497e-07	0.9	-0.4	0.4	0.2	0.3	0.108	0.3733	0.0094	0.0043
0.0348	3.48	0.458	1.686e-07	0.7	-0.2	0.6	0.7	0.4	0.108	0.3825	0.0076	0.0047
0.0354	4.41	0.568	9.558e-08	0.6	0.0	0.8	1.5	0.5	0.108	0.3825	0.0103	0.0070
0.0374	5.32	0.645	6.281e-08	0.5	0.0	1.0	2.0	0.6	0.108	0.4031	0.0278	0.0094
0.0497	2.54	0.237	2.342e-07	1.2	-0.6	0.2	0.1	0.2	0.117	0.3394	0.0087	0.0048
0.0494	3.49	0.327	1.288e-07	0.9	-0.4	0.2	0.3	0.3	0.117	0.3785	0.0070	0.0043
0.0495	4.47	0.416	7.061e-08	0.8	-0.2	0.3	0.7	0.3	0.117	0.3681	0.0073	0.0043
0.0504	5.43	0.493	4.448e-08	0.7	-0.1	0.5	1.0	0.4	0.117	0.3705	0.0099	0.0050
0.0524	6.61	0.576	3.014e-08	0.6	0.0	0.7	1.2	0.5	0.117	0.4086	0.0162	0.0065
0.0707	2.56	0.168	1.725e-07	1.5	-0.9	0.3	0.1	0.2	0.113	0.3426	0.0129	0.0061
0.0702	3.50	0.229	9.223e-08	1.2	-0.6	0.3	0.2	0.2	0.113	0.3584	0.0089	0.0051
0.0698	4.48	0.295	5.437e-08	1.0	-0.4	0.3	0.3	0.2	0.113	0.3659	0.0089	0.0043
0.0700	5.47	0.357	3.656e-08	0.9	-0.3	0.3	0.4	0.3	0.113	0.3867	0.0106	0.0040
0.0700	6.86	0.448	2.175e-08	0.7	-0.1	0.4	0.7	0.4	0.113	0.3902	0.0130	0.0047
0.0718	8.62	0.544	1.460e-08	0.6	0.0	1.1	0.5	0.113	0.4555	0.0308	0.0068	
0.0915	2.61	0.132	1.515e-07	1.8	-1.2	0.2	0.0	0.2	0.096	0.3948	0.0202	0.0089
0.0909	3.50	0.177	7.095e-08	1.4	-0.8	0.3	0.1	0.2	0.096	0.3430	0.0109	0.0058
0.0906	4.47	0.226	4.441e-08	1.2	-0.6	0.4	0.2	0.2	0.096	0.3645	0.0108	0.0051
0.0904	5.48	0.278	2.948e-08	1.0	-0.4	0.4	0.2	0.2	0.096	0.3807	0.0120	0.0047
0.0904	6.81	0.343	1.812e-08	0.9	-0.3	0.5	0.4	0.3	0.096	0.3814	0.0112	0.0043
0.0905	8.77	0.440	1.099e-08	0.7	-0.1	0.7	0.7	0.4	0.096	0.4158	0.0221	0.0054
0.1126	2.62	0.109	9.990e-08	2.2	-1.5	0.2	0.0	0.2	0.043	0.3174	0.0196	0.0082
0.1120	3.48	0.143	6.469e-08	1.7	-1.1	0.3	0.1	0.2	0.043	0.3721	0.0165	0.0078
0.1111	4.48	0.185	3.714e-08	1.4	-0.8	0.4	0.1	0.2	0.043	0.3654	0.0132	0.0059
0.1109	5.49	0.227	2.441e-08	1.2	-0.6	0.4	0.1	0.2	0.043	0.3718	0.0134	0.0050
0.1109	6.83	0.281	1.473e-08	1.0	-0.4	0.6	0.2	0.2	0.043	0.3646	0.0117	0.0045
0.1106	8.87	0.365	9.308e-09	0.8	-0.2	0.8	0.4	0.3	0.043	0.4145	0.0209	0.0053
0.1112	10.76	0.437	4.964e-09	0.7	-0.1	1.1	0.6	0.4	0.043	0.3462	0.0357	0.0050
0.1435	3.48	0.113	4.974e-08	2.0	-1.4	0.3	0.0	0.2	0.231	0.3610	0.0134	0.0088
0.1421	4.49	0.147	2.726e-08	1.6	-1.0	0.2	0.0	0.2	0.198	0.3364	0.0102	0.0062
0.1411	5.48	0.179	1.738e-08	1.4	-0.8	0.3	0.1	0.2	0.175	0.3258	0.0101	0.0051
0.1413	6.87	0.224	1.128e-08	1.2	-0.5	0.5	0.1	0.2	0.151	0.3459	0.0087	0.0047
0.1407	8.90	0.291	6.779e-09	1.0	-0.3	0.8	0.2	0.2	0.130	0.3682	0.0147	0.0050
0.1423	11.01	0.352	4.435e-09	0.8	-0.2	1.1	0.3	0.3	0.115	0.3925	0.0215	0.0057
0.1821	3.62	0.092	3.152e-08	2.3	-1.6	0.7	0.0	0.2	0.204	0.3116	0.0180	0.0091
0.1866	4.50	0.113	2.134e-08	1.9	-1.2	0.3	0.0	0.2	0.175	0.3403	0.0126	0.0076
0.1845	5.49	0.137	1.336e-08	1.6	-0.9	0.1	0.0	0.2	0.153	0.3198	0.0119	0.0060
0.1837	6.87	0.172	8.988e-09	1.3	-0.7	0.4	0.1	0.2	0.132	0.3461	0.0101	0.0053
0.1813	8.94	0.227	4.992e-09	1.1	-0.4	0.8	0.1	0.2	0.113	0.3361	0.0159	0.0047
0.1816	11.15	0.280	3.358e-09	0.9	-0.3	1.1	0.2	0.2	0.099	0.3692	0.0196	0.0054
0.2292	4.56	0.093	1.562e-08	1.9	-1.3	0.3	0.0	0.2	0.158	0.3112	0.0149	0.0072
0.2312	5.47	0.110	1.054e-08	1.7	-1.0	0.2	0.0	0.2	0.139	0.3104	0.0126	0.0061
0.2311	6.92	0.139	6.614e-09	1.4	-0.7	0.5	0.0	0.2	0.118	0.3188	0.0099	0.0051
0.2276	8.84	0.178	3.854e-09	1.1	-0.5	0.8	0.1	0.2	0.101	0.3082	0.0129	0.0046
0.2276	11.24	0.226	2.722e-09	1.0	-0.3	1.1	0.1	0.2	0.087	0.3664	0.0184	0.0054
0.2801	5.54	0.093	8.133e-09	1.5	-0.8	0.8	0.0	0.2	0.127	0.2960	0.0161	0.0054
0.2853	6.93	0.113	4.854e-09	1.2	-0.5	0.9	0.0	0.2	0.107	0.2866	0.0106	0.0049
0.2808	8.86	0.146	3.030e-09	1.0	-0.3	1.1	0.0	0.2	0.091	0.2946	0.0140	0.0046
0.2790	11.27	0.186	1.738e-09	0.9	-0.2	1.3	0.1	0.2	0.078	0.2814	0.0164	0.0046
0.2792	14.19	0.231	1.114e-09	0.8	0.0	1.5	0.1	0.2	0.068	0.2971	0.0295	0.0051
0.3411	7.08	0.097	3.646e-09	0.5	0.2	2.3	0.0	0.2	0.099	0.2675	0.0104	0.0063
0.3527	8.86	0.117	2.095e-09	0.5	0.3	2.1	0.0	0.2	0.083	0.2532	0.0104	0.0056
0.3528	11.33	0.149	1.152e-09	0.5	0.4	2.0	0.1	0.2	0.070	0.2340	0.0117	0.0048
0.3521	14.32	0.186	7.875e-10	0.5	0.4	1.9	0.1	0.2	0.060	0.2631	0.0197	0.0053
0.4334	9.02	0.097	1.050e-09	-2.5	3.4	6.8	0.0	0.2	0.077	0.1610	0.0103	0.0128
0.4626	11.36	0.115	6.386e-10	-2.0	3.0	4.7	0.0	0.2	0.064	0.1692	0.0095	0.0099
0.4722	14.39	0.141	3.458e-10	-1.5	2.6	2.7	0.0	0.2	0.054	0.1535	0.0115	0.0063

Table 3: (b) The differential scattering cross section, $d^2 \frac{m}{p} \text{eas} = dx dQ^2$, the value of R as used in the analysis (see also table 7), and the structure function F_2^p at 120 GeV incident muon energy, with the normalisation corrections of table 2. Horizontal lines separate the x-bins. See also caption (a).

(continued)							
x	Q^2 (GeV 2)	R	F_2^P	F_2^{stat}	F_2^{syst}	R_{1990}	F_2^P
0.1400	1.75	0.295	0.3688	0.0220	0.0138	0.295	0.3672
0.1400	2.50	0.270	0.3630	0.0071	0.0101	0.270	0.3619
0.1400	3.50	0.232	0.3685	0.0063	0.0073	0.232	0.3678
0.1400	4.50	0.200	0.3540	0.0064	0.0057	0.200	0.3536
0.1400	5.50	0.175	0.3410	0.0076	0.0050	0.175	0.3407
0.1400	7.00	0.150	0.3542	0.0070	0.0051	0.150	0.3540
0.1400	9.00	0.129	0.3775	0.0114	0.0060	0.129	0.3774
0.1400	11.50	0.114	0.3737	0.0092	0.0068	0.114	0.3736
0.1400	15.00	0.100	0.3700	0.0067	0.0074	0.100	0.3699
0.1400	20.00	0.089	0.3650	0.0054	0.0078	0.089	0.3649
0.1400	27.00	0.079	0.3746	0.0059	0.0090	0.079	0.3743
0.1400	36.00	0.072	0.3642	0.0100	0.0103	0.072	0.3635
0.1800	2.50	0.251	0.3628	0.0109	0.0114	0.251	0.3619
0.1800	3.50	0.210	0.3343	0.0074	0.0082	0.210	0.3336
0.1800	4.50	0.178	0.3609	0.0079	0.0071	0.178	0.3604
0.1800	5.50	0.155	0.3277	0.0084	0.0055	0.155	0.3273
0.1800	7.00	0.132	0.3461	0.0078	0.0053	0.132	0.3459
0.1800	9.00	0.113	0.3468	0.0119	0.0056	0.113	0.3467
0.1800	11.50	0.098	0.3527	0.0111	0.0062	0.098	0.3526
0.1800	15.00	0.085	0.3382	0.0081	0.0069	0.085	0.3382
0.1800	20.00	0.075	0.3392	0.0062	0.0073	0.075	0.3391
0.1800	27.00	0.066	0.3413	0.0063	0.0081	0.066	0.3411
0.1800	36.00	0.059	0.3548	0.0083	0.0096	0.059	0.3545
0.1800	48.00	0.054	0.3715	0.0157	0.0114	0.054	0.3708
0.2250	2.50	0.234	0.3330	0.0315	0.0101	0.234	0.3322
0.2250	3.50	0.191	0.3297	0.0087	0.0082	0.191	0.3291
0.2250	4.50	0.161	0.3213	0.0078	0.0065	0.161	0.3208
0.2250	5.50	0.140	0.3318	0.0090	0.0058	0.140	0.3315
0.2250	7.00	0.118	0.3217	0.0078	0.0048	0.118	0.3215
0.2250	9.00	0.100	0.3117	0.0104	0.0049	0.100	0.3116
0.2250	11.50	0.086	0.3485	0.0112	0.0063	0.086	0.3484
0.2250	15.00	0.074	0.3149	0.0081	0.0064	0.074	0.3150
0.2250	20.00	0.064	0.3080	0.0059	0.0065	0.064	0.3080
0.2250	27.00	0.056	0.3164	0.0061	0.0072	0.056	0.3164
0.2250	36.00	0.050	0.3031	0.0071	0.0076	0.050	0.3030
0.2250	48.00	0.045	0.3166	0.0121	0.0089	0.045	0.3163
0.2750	3.50	0.178	0.3016	0.0147	0.0076	0.178	0.3011
0.2750	4.50	0.149	0.3036	0.0101	0.0060	0.149	0.3033
0.2750	5.50	0.129	0.3032	0.0101	0.0051	0.129	0.3029
0.2750	7.00	0.108	0.3035	0.0086	0.0049	0.108	0.3033
0.2750	9.00	0.091	0.3031	0.0125	0.0047	0.091	0.3031
0.2750	11.50	0.078	0.2789	0.0113	0.0050	0.078	0.2789
0.2750	15.00	0.066	0.2933	0.0111	0.0055	0.066	0.2934
0.2750	20.00	0.056	0.2828	0.0066	0.0058	0.056	0.2829
0.2750	27.00	0.048	0.2645	0.0061	0.0056	0.048	0.2647
0.2750	36.00	0.042	0.2817	0.0073	0.0064	0.042	0.2818
0.2750	48.00	0.038	0.2764	0.0113	0.0068	0.038	0.2764
0.2750	65.00	0.034	0.1887	0.0289	0.0055	0.034	0.1886
0.3500	4.50	0.138	0.2727	0.0116	0.0127	0.138	0.2725
0.3500	5.50	0.119	0.2526	0.0093	0.0092	0.119	0.2524
0.3500	7.00	0.099	0.2690	0.0073	0.0063	0.099	0.2689
0.3500	9.00	0.083	0.2490	0.0088	0.0055	0.083	0.2489
0.3500	11.50	0.070	0.2354	0.0118	0.0048	0.070	0.2354
0.3500	15.00	0.059	0.2192	0.0081	0.0045	0.059	0.2193
0.3500	20.00	0.049	0.2257	0.0058	0.0045	0.049	0.2258
0.3500	27.00	0.042	0.2156	0.0044	0.0046	0.042	0.2158
0.3500	36.00	0.036	0.2163	0.0048	0.0054	0.036	0.2165
0.3500	48.00	0.032	0.2207	0.0065	0.0061	0.032	0.2209
0.3500	65.00	0.028	0.2333	0.0192	0.0074	0.028	0.2335
0.5000	5.50	0.109	0.1558	0.0158	0.0182	0.109	0.1557
0.5000	7.00	0.091	0.1654	0.0077	0.0161	0.091	0.1653
0.5000	9.00	0.075	0.1377	0.0063	0.0107	0.075	0.1376
0.5000	11.50	0.063	0.1443	0.0081	0.0085	0.063	0.1443
0.5000	15.00	0.052	0.1344	0.0101	0.0055	0.052	0.1344
0.5000	20.00	0.043	0.1192	0.0059	0.0050	0.043	0.1193
0.5000	27.00	0.035	0.1185	0.0035	0.0051	0.035	0.1186
0.5000	36.00	0.030	0.1112	0.0028	0.0049	0.030	0.1114
0.5000	48.00	0.026	0.1042	0.0034	0.0049	0.026	0.1044
0.5000	65.00	0.022	0.1092	0.0088	0.0057	0.022	0.1094

Table 5: The structure function F_2^P averaged over measurements for all energies and both triggers with the normalisation corrections of table 2. The results are the statistically weighted averages given at the centre of each $(x; Q^2)$ -bin. The values of R are those used in the analysis. In the last column we give the values of F_2^P obtained using the values of R_{1990} taken from the parametrisation of ref. [2].

(continued)

x	Q^2 (GeV 2)	R	F_2^d	F_2^{stat}	F_2^{syst}	R ₁₉₉₀	F_2^d
0.1400	1.75	0.295	0.3471	0.0198	0.0168	0.295	0.3458
0.1400	2.50	0.270	0.3294	0.0060	0.0104	0.270	0.3285
0.1400	3.50	0.232	0.3302	0.0050	0.0067	0.232	0.3295
0.1400	4.50	0.200	0.3212	0.0050	0.0050	0.200	0.3207
0.1400	5.50	0.175	0.3291	0.0059	0.0047	0.175	0.3286
0.1400	7.00	0.150	0.3246	0.0051	0.0047	0.150	0.3242
0.1400	9.00	0.129	0.3410	0.0082	0.0054	0.129	0.3407
0.1400	11.50	0.114	0.3280	0.0066	0.0059	0.114	0.3278
0.1400	15.00	0.100	0.3326	0.0049	0.0061	0.100	0.3324
0.1400	20.00	0.089	0.3307	0.0039	0.0059	0.089	0.3305
0.1400	27.00	0.079	0.3322	0.0040	0.0060	0.079	0.3319
0.1400	36.00	0.072	0.3421	0.0067	0.0071	0.072	0.3416
0.1800	2.50	0.251	0.3267	0.0091	0.0103	0.251	0.3259
0.1800	3.50	0.210	0.3062	0.0061	0.0073	0.210	0.3056
0.1800	4.50	0.178	0.3121	0.0060	0.0057	0.178	0.3116
0.1800	5.50	0.155	0.3015	0.0064	0.0048	0.155	0.3011
0.1800	7.00	0.132	0.3059	0.0056	0.0044	0.132	0.3056
0.1800	9.00	0.113	0.3014	0.0084	0.0045	0.113	0.3011
0.1800	11.50	0.098	0.3061	0.0078	0.0049	0.098	0.3058
0.1800	15.00	0.085	0.3081	0.0061	0.0057	0.085	0.3079
0.1800	20.00	0.075	0.2992	0.0043	0.0057	0.075	0.2991
0.1800	27.00	0.066	0.3021	0.0043	0.0061	0.066	0.3019
0.1800	36.00	0.059	0.3016	0.0053	0.0067	0.059	0.3013
0.1800	48.00	0.054	0.3207	0.0099	0.0081	0.054	0.3204
0.2250	2.50	0.234	0.2939	0.0260	0.0080	0.234	0.2934
0.2250	3.50	0.191	0.2904	0.0070	0.0065	0.191	0.2899
0.2250	4.50	0.161	0.2796	0.0060	0.0052	0.161	0.2792
0.2250	5.50	0.140	0.2853	0.0066	0.0046	0.140	0.2849
0.2250	7.00	0.118	0.2799	0.0056	0.0038	0.118	0.2796
0.2250	9.00	0.100	0.2798	0.0075	0.0038	0.100	0.2795
0.2250	11.50	0.086	0.2876	0.0077	0.0041	0.086	0.2874
0.2250	15.00	0.074	0.2614	0.0057	0.0043	0.074	0.2612
0.2250	20.00	0.064	0.2695	0.0042	0.0046	0.064	0.2693
0.2250	27.00	0.056	0.2688	0.0041	0.0053	0.056	0.2685
0.2250	36.00	0.050	0.2599	0.0047	0.0058	0.050	0.2598
0.2250	48.00	0.045	0.2611	0.0075	0.0071	0.045	0.2610
0.2750	3.50	0.178	0.2667	0.0117	0.0062	0.178	0.2664
0.2750	4.50	0.149	0.2656	0.0078	0.0051	0.149	0.2652
0.2750	5.50	0.129	0.2581	0.0074	0.0041	0.129	0.2578
0.2750	7.00	0.108	0.2481	0.0059	0.0033	0.108	0.2478
0.2750	9.00	0.091	0.2471	0.0083	0.0029	0.091	0.2469
0.2750	11.50	0.078	0.2402	0.0079	0.0030	0.078	0.2400
0.2750	15.00	0.066	0.2439	0.0078	0.0031	0.066	0.2437
0.2750	20.00	0.056	0.2347	0.0046	0.0031	0.056	0.2346
0.2750	27.00	0.048	0.2284	0.0041	0.0035	0.048	0.2283
0.2750	36.00	0.042	0.2311	0.0047	0.0046	0.042	0.2310
0.2750	48.00	0.038	0.2347	0.0071	0.0060	0.038	0.2347
0.2750	65.00	0.034	0.1704	0.0183	0.0057	0.034	0.1704
0.3500	4.50	0.138	0.2123	0.0081	0.0093	0.138	0.2120
0.3500	5.50	0.119	0.2192	0.0069	0.0074	0.119	0.2187
0.3500	7.00	0.099	0.2153	0.0049	0.0046	0.099	0.2149
0.3500	9.00	0.083	0.2014	0.0058	0.0027	0.083	0.2010
0.3500	11.50	0.070	0.1842	0.0074	0.0019	0.070	0.1839
0.3500	15.00	0.059	0.1716	0.0053	0.0022	0.059	0.1714
0.3500	20.00	0.049	0.1819	0.0039	0.0028	0.049	0.1818
0.3500	27.00	0.042	0.1706	0.0028	0.0029	0.042	0.1705
0.3500	36.00	0.036	0.1728	0.0030	0.0030	0.036	0.1728
0.3500	48.00	0.032	0.1659	0.0038	0.0032	0.032	0.1659
0.3500	65.00	0.028	0.1580	0.0105	0.0047	0.028	0.1580
0.5000	5.50	0.109	0.1158	0.0101	0.0122	0.109	0.1155
0.5000	7.00	0.091	0.1237	0.0047	0.0102	0.091	0.1232
0.5000	9.00	0.075	0.1046	0.0039	0.0064	0.075	0.1042
0.5000	11.50	0.063	0.1025	0.0046	0.0049	0.063	0.1021
0.5000	15.00	0.052	0.1077	0.0061	0.0040	0.052	0.1074
0.5000	20.00	0.043	0.0901	0.0037	0.0043	0.043	0.0899
0.5000	27.00	0.035	0.0864	0.0021	0.0045	0.035	0.0863
0.5000	36.00	0.030	0.0828	0.0017	0.0041	0.030	0.0827
0.5000	48.00	0.026	0.0810	0.0020	0.0037	0.026	0.0810
0.5000	65.00	0.022	0.0729	0.0047	0.0032	0.022	0.0729

Table 6: The structure function F_2^d averaged over measurements for all energies and both triggers with the normalisation corrections of table 2. The results are the statistically weighted averages given at the centre of each $(x; Q^2)$ -bin. The values of R are those used in the analysis. In the last column we give the values of F_2^d obtained using the values of R₁₉₉₀ taken from the parametrisation of ref. [2].